J Appl Physiol 114: 665–674, 2013.
First published January 3, 2012; doi:10.1152/japplphysiol.00661.2012.

Dust from hog confinement facilities impairs Ca^{2+} mobilization from sarco(endo)plasmic reticulum by inhibiting ryanodine receptors

Chengju Tian,[1] Caronda J. Moore,[1] Puttappa Dodmane,[1] Chun Hong Shao,[1] Debra J. Romberger,[4,2,3] Myron L. Toews,[1] and Keshore R. Bidasee[1,3,5]

[1]*Department of Pharmacology and Experimental Neuroscience, University of Nebraska Medical Center, Omaha, Nebraska;* [2]*Department of Internal Medicine, Pulmonary and Critical Care Medicine Section, University of Nebraska Medical Center, Omaha, Nebraska;* [3]*Department of Environmental, Agricultural and Occupational Health, University of Nebraska Medical Center, Omaha, Nebraska;* [4]*VA Nebraska Western Iowa Healthcare System, Omaha, Nebraska; and* [5]*Nebraska Center for Redox Biology, Lincoln, Nebraska*

Submitted 1 June 2012; accepted in final form 31 December 2012

Tian C, Moore CJ, Dodmane P, Shao CH, Romberger DJ, Toews ML, Bidasee KR. Dust from hog confinement facilities impairs Ca^{2+} mobilization from sarco(endo)plasmic reticulum by inhibiting ryanodine receptors. *J Appl Physiol* 114: 665–674, 2013. First published January 3, 2012; doi:10.1152/japplphysiol.00661.2012.— Individuals working in commercial hog confinement facilities have elevated incidences of headaches, depression, nausea, skeletal muscle weakness, fatigue, gastrointestinal disorders, and cardiovascular diseases, and the molecular mechanisms for these nonrespiratory ailments remain incompletely undefined. A common element underlying these diverse pathophysiologies is perturbation of intracellular Ca^{2+} homeostasis. This study assessed whether the dust generated inside hog confinement facilities contains compounds that alter Ca^{2+} mobilization via ryanodine receptors (RyRs), key intracellular channels responsible for mobilizing Ca^{2+} from internal stores to elicit an array of physiologic functions. Hog barn dust (HBD) was extracted with phosphate-buffered saline, sterile-filtered (0.22 μm), and size-separated using Sephadex G-100 resin. Fractions (F) 1 through 9 (M_w >10,000 Da) had no measurable effects on RyR isoforms. However, F10 through F17, which contained compounds of M_w ≤2,000 Da, modulated the [^{3}H]ryanodine binding to RyR1, RyR2, and RyR3 in a biphasic (Gaussian) manner. The K_i values for F13, the most potent fraction, were 3.8 ± 0.2 μg/ml for RyR1, 0.2 ± 0.01 μg/ml and 19.1 ± 2.8 μg/ml for RyR2 (two binding sites), and 44.9 ± 2.8 μg/ml and 501.6 ± 9.2 μg/ml for RyR3 (two binding sites). In lipid bilayer assays, F13 dose-dependently decreased the open probabilities of RyR1, RyR2, and RyR3. Pretreating differentiated mouse skeletal myotubes (C2C12 cells) with F13 blunted the amplitudes of ryanodine- and K^+-induced Ca^{2+} transients. Because RyRs are present in many cell types, impairment in Ca^{2+} mobilization from internal stores via these channels is a possible mechanism by which HBD may trigger these seemingly unrelated pathophysiologies.

intracellular Ca^{2+} homeostasis; cardiovascular diseases and nonrespiratory ailments

CONCENTRATED ANIMAL FEEDING operations (CAFOs) are widely used in the United States and other industrialized countries to raise pigs for commercial production of pork and pork products (8, 34, 47). To reach market size in a timely and predictable manner, pigs housed in these facilities are fed a standardized diet rich in protein and containing growth hormones, vitamins, and antibiotics (28). Particulate matter generated from the feed combines with feces, urine, dander, microbes, volatile substances, and gases to produce what is referred to as hog barn dust (HBD) (15, 51). The majority of HBD generated inside hog confinement facilities is vented out into the environment via a negative pressure ventilation system (8, 27, 42, 47). The rest circulates or settles on ledges inside the facilities. Individuals who work inside hog CAFOs are exposed to HBD on a daily basis and concerted efforts are ongoing to delineate and ameliorate the impact of HBD on the health of these individuals. Individuals living in facilities in close proximity to CAFOs may also be exposed to high levels of HBD on a daily basis. However, the extent to which the latter occurs and its clinical consequences are not well documented.

Numerous studies have pointed to inhalation of HBD as a contributing cause for the increased incidence of respiratory illnesses in individuals working inside hog CAFOs, including shortness of breath, wheezing, coughing, chest tightness, asthma-like syndrome, chronic bronchitis, and chronic obstructive pulmonary diseases (22, 23, 25, 30, 33, 43, 45, 50). Activation of macrophages, protein kinase C, and toll-like receptors; increased production and release of inflammatory mediators (IL-6, IL-8, and TNF-α); and increased adhesion of peripheral blood lymphocytes to bronchial epithelial cells are mechanisms that have been implicated in HBD-induced respiratory illnesses (1, 34, 39, 40, 44). Less clear is whether the plethora of nonrespiratory ailments, including headaches, depression, skeletal muscle aches and fatigue, nausea, gastrointestinal disorders, and exacerbation of existing cardiovascular diseases including heart failure and arrhythmias, are secondary consequences of the respiratory ailments from HBD or stem from the direct actions HBD on other cells and organs (11, 16, 17, 23, 41).

A transient rise in intracellular Ca^{2+} is used by many cell types as a signal to activate an array of important physiologic functions, including hormone secretion, neurotransmitter release, muscle contraction, gene expression, cell proliferation, and apoptosis (3). A significant percentage of this signaling Ca^{2+} is mobilized from internal Ca^{2+} stores, known as the sarco(endo)plasmic reticulum (SR/ER) via Ca^{2+}-release channels. The inability of cells to recruit Ca^{2+} from the SR/ER not only reduces the amplitude of the desired physiological responses but can also cause an array of adverse effects that include headaches, diarrhea, nausea, muscle weakness, and fatigue (12, 13, 35).

Two classes of Ca^{2+}-release channels reside on the SR/ER membranes, ryanodine receptors (RyRs) and inositol, 1,4,5-trisphosphate receptors (IP_3Rs) (5, 18). RyRs are significantly larger in size than IP_3Rs (2.5×10^6 Da vs. 0.8×10^6 Da) and recruit ~20 times more Ca^{2+} from the SR/ER compared with IP_3Rs (31). Unlike IP_3Rs, RyRs are directly activated by a rise in

Address for reprint requests and other correspondence: K.R. Bidasee, 985800 Nebraska Medical Center, Durham Research Center, DRC 3047, Omaha, NE 68198-5800 (e-mail: kbidasee@unmc.edu).

intracellular Ca^{2+}. Three isoforms of RyRs are expressed in mammalian cells. Type 1 ryanodine receptor (RyR1) is predominant in skeletal muscle but is also found in the diaphragm and colonic epithelial cells. Type 2 ryanodine receptor (RyR2) is the major Ca^{2+}-release channel in the heart and brain. Type 3 ryanodine receptor (RyR3) is present in the diaphragm and vascular and gastrointestinal smooth muscle cells (12, 19). Defects in function of RyRs leads to an array of diseases, including malignant hyperthermia, central core disease, stress-induced catecholaminergic polymorphic ventricular tachycardia, and arrhythmogenic right ventricular dysplasia (13, 29). Alterations in RyR function also play important roles in the pathogenesis of Alzheimer's disease, neurocognitive impairment, and nausea (26, 55). Antibodies against RyR are found in individuals with myasthenia gravis (43), suggesting a role for these receptors in the disease.

Recently we found that chloroform extracts of HBD contain compounds that bind to and modulate RyR1 (48). In another study we found that aqueous extracts of HBD also increase intracellular Ca^{2+} in airway epithelial cells, but the mechanisms responsible for the latter remain unknown (14). Because of their importance in elevating cytoplasmic Ca^{2+} needed to execute cellular functions in a diverse array of cells, this study was designed to investigate whether the aqueous extracts of HBD contain compounds that can bind to and modulate the activities of one or more of the three isoforms of RyR; namely, RyR1, RyR2, and RyR3.

MATERIAL AND METHODS

MATERIALS

[^{3}H]Ryanodine (specific activity 87 Ci/mmol) was purchased from GE Life Sciences (Boston, MA). Phosphatidylserine, phosphatidylcholine, and phosphatidylethanolamine were obtained from Avanti Polar Lipids (Alabaster, AL). Dialysis membranes were obtained from Spectrum Laboratories (Rancho Dominguez, CA). All other reagents and solvents used were of the highest grade commercially available.

Extraction of HBD

HBD collected 1–2 meters above the floor from hog confinement facilities in central Nebraska was extracted using HEPES-buffered saline (1 g HBD in 10 ml for 1 h at room temperature with continuous mixing). Extracts were centrifuged three times at 13,000 $\times$ g_{av} to remove particulate material, filtered through 0.22-μm membranes to remove microbes, and stored at -20°C until use. This material is referred to as HBD_{aq}.

Fractionation of HBD_{aq}

HBD_{aq} was separated into fractions of varying molecular sizes using Sephadex G-100 resin. Sephadex G-100 (10 g) beads were activated by dissolving in phosphate-buffered saline (PBS) containing 0.5% BSA for 16 h at 4°C. Activated beads were poured into a glass column (49 cm height, 1.5 cm diameter) and washed with PBS (300 ml). HBD_{aq} (2.5 ml) was then loaded onto the column and eluted with PBS at a flow rate of 0.33 ml/min. A mixture of BSA (66 kDa), carbonic anhydrase (29 kDa), cytochrome C (12.4 kDa), and epidermal growth factor (EGF, 6.5 kDa) was used to estimate sizes of compounds present in the fractions. Following elution of the column void volume, continuous 6-ml fractions were collected in preweighed vials, labeled as F1 through F17, and freeze-dried. After freeze-drying, the vials were reweighed, with the freeze-dried mass of an equal volume of PBS subtracted to determine the mass of HBD in each fraction.

Preparation of Membrane Vesicles

The Institutional Animal Care and Use Committee of the University of Nebraska Medical Center approved the use of rabbits (male New Zealand) and rats (male Sprague Dawley) for this study, and their short-term housing adhered to the Institute for Laboratory Animal Research *Guide for Care and Use of Laboratory Animals* (37).

RyR1. SR vesicles were prepared from the fast-twitch muscles of male New Zealand white rabbits as described previously (48). After deep anesthesia with Inactin (150 mg/kg via an ear vein), fast-twitch muscles from hind legs were removed, placed in isolation buffer [0.3 M sucrose, 10 mM imidazole·HCl, 230 μM phenylmethylsulfonyl fluoride (PMSF), 1.1 μM leupeptin pH 7.4], homogenized (3 $\times$ 10 s, speed setting 4.5, ProScientific, Oxford, CT), and centrifuged at 7,500 $\times$ g_{av} for 20 min. The supernatant was discarded and the pellet was resuspended in fresh isolation buffer, homogenized a second time at speed setting 5.5, and centrifuged at 11,000 $\times$ g_{av} for 20 min. The supernatant was then filtered through cheesecloth, and SR vesicles were obtained by sedimentation at 85,000 $\times$ g_{av} for 30 min.

RyR2. SR membrane vesicles were prepared from rat heart as described earlier (49). After deep anesthesia with Inactin, hearts from 15 rats were removed and placed into ice-cold saline solution. Atrial tissues were removed and ventricles were homogenized in a buffer consisting of 10 mM $NaHCO_3$, 230 μM PMSF, and 1.1 μM leupeptin pH 7.4 (speed setting 4.5, 3 $\times$ 6 s). Homogenates were then centrifuged at 12,000 $\times$ g_{av} for 20 min to remove mitochondria and nuclear debris. The supernatant was centrifuged at 46,000 $\times$ g_{av} for 30 min and the pellet (SR membranes) was resuspended in buffer containing 0.25 M sucrose, 10 mM histidine, 230 μM PMSF, and 1.1 μM leupeptin pH 7.4, quick-frozen, and stored at -80°C until use.

RyR3. Complementary DNA encoding RyR3 (10–15 μg, a gift from Dr. Wayne Chen, University of Alberta, Edmonton, AB) was transfected into HEK-293T cells (sixteen 100-mm dishes at 30–40% confluency grown in Dulbecco's modified Eagle's medium using the calcium phosphate method (10). Six hours after transfection, medium was replaced and cells were grown for an additional 36–44 h. Cells were then washed with 1$\times$ PBS containing 1 mM EDTA; harvested by centrifugation (500 $\times$ g_{av} for 3 min); resuspended in buffer containing 0.25 M sucrose, 10 mM histidine pH 7.3, and a protease inhibitor mix (1 mM benzamidine, 2 μg/ml leupeptin, 2 μg/ml pepstatin A, 2 μg/ml aprotinin, and 0.5 mM PMSF); and homogenized (3 $\times$ 6 s). Homogenates were centrifuged (85,000 $\times$ g_{av} for 45 min) and SR membranes were collected, quick-frozen in liquid nitrogen, and stored at -80°C.

Preparation of Junctional SR Membranes

Junctional SR membranes containing RyR1 were prepared by fractionating SR membranes using discontinuous sucrose (0.6 M, 0.8 M, 1.2 M, 1.5 M) gradient centrifugation (103,745 $\times$ g_{av} for 2 h) and collecting membranes at the 1.2–1.5 M sucrose interface (48). Junctional SR membranes containing RyR2 were prepared by fractionating SR membranes using discontinuous sucrose (0.6 M, 0.8 M, 1.0 M, 1.5 M) gradient centrifugation (103,745 $\times$ g_{av} for 2 h) and collecting membranes at the 1.0–1.5 M sucrose interface (49).

Preparation of Proteoliposomes Containing RyR

Proteoliposomes containing RyR1 and RyR2 were prepared as described previously (48, 49). For preparation of proteoliposomes containing RyR3, 3.0 mg/ml of HEK-293T cell membranes were solubilized with 1.5% 3-[(3-cholamidopropyl)dimethylammonio]-1-propanesulfonate. Proteoliposomes were stored in the vapor phase of a liquid nitrogen freezer until use.

[^{3}H]Ryanodine Binding Assays

Identification of sephadex G100 fractions that bind to RyRs. SR membranes (0.1 mg/ml) containing RyR1, RyR2, or RyR3 were

incubated in binding buffer (500 mM KCl, 20 mM Tris-HCl, 0.4 mM $CaCl_2$, 0.1 mM EGTA pH 7.4) containing 6.7 nM [^{3}H]ryanodine and 75 or 150 μg/ml of fractions F1 through F17 for 2 h at 37°C. Ryanodine (1 μM) and HEPES-buffered saline (1%) were used as controls. At the end of the incubation, samples were rapidly filtered through GF/C filters using a cell harvester (Brandel, Gaithersburg, MD), washed three times with ice-cold binding buffer (3 ml), and the amount of [^{3}H]ryanodine bound to the filters was quantified by liquid scintillation counting (7).

Determination of IC_{50} and K_i of F13. Competition for high-affinity [^{3}H]ryanodine binding was used to determine IC_{50} and K_i values for binding of the most active fraction, F13, to RyR1, RyR2, and RyR3. F13 concentrations ranging from 1 to 8,000 μg/ml were used. For determination of IC_{50} values, competition data were fitted to one- and two-site models using nonlinear regression analysis (36). The Cheng-Prusoff equation [$K_i = IC_{50}/(1 + (L/K_L)$] was used to determine the K_i values for F13 on binding to RyR1, RyR2, and RyR3, where L is the concentration of [^{3}H]ryanodine (6.7 nM) and K_L is the equilibrium dissociation constant of [^{3}H]ryanodine (2.4 nM for RyR1, 1.2 nM for RyR2, and 3.6 nM for RyR3) (7, 49).

Single-Channel Measurement and Analyses

Lipid bilayer assays were used to determine the functional consequences of F13 on binding to RyR1, RyR2, and RyR3 (48, 49). Phosphatidylethanolamine, phosphatidylserine, and phosphatidylcholine in a ratio of 5:3:2 (35 mg/ml of lipid) in *n*-decane were painted across the 200-μm diameter hole of a bilayer cup. Purified RyR1, RyR2, or RyR3 was then incorporated into the lipid bilayer for single-channel assays. The side of the bilayer to which proteoliposomes were added was designated as the *cis* side, the opposite side as *trans* or ground. F13 was added to the *cis* chamber and vigorously stirred for ~30 s. Channel activity was then recorded for 6 min (3 min at +35 mV and 3 min at −35 mV) in symmetric KCl buffer (0.25 mM KCl, 20 mM K-HEPES pH 7.4) with 3.3 μM or 9.2 μM Ca^{2+} in the *cis* chamber. Electrical signals were filtered at 2 kHz, digitized at 10 kHz, and analyzed using pClamp (Molecular Devices, Sunnyvale, CA). All assays were conducted at room temperature (23–25°C) in ambient oxygen.

Effects of F13 on Ca^{2+} Mobilization from Sarco(endo)plasmic Reticulum via RyRs in Quiescent Cells

Mouse skeletal muscle myoblasts (C2C12 cells) were grown on laminin-coated glass-bottomed chambers in DMEM containing 1.8 mM $CaCl_2$ supplemented with 2% fetal bovine serum and antibiotics (100 units/ml penicillin, 100 μg/ml streptomycin, and 100 μg/ml gentamicin pH 7.3) to allow differentiation. At 60–70% confluency, differentiated myotubes were loaded with Fluo 3-AM (5 μM for 30 min at 37°C), washed, switched to DMEM without $CaCl_2$, and placed on the stage of a laser confocal microscope (Zeiss LSM 510 equipped with an Argon-Krypton Laser, 25 mW argon laser, 488 nm, 1% intensity, Thornwood, NJ; Plan-Apochromat 63×/1.4 oil lens, pinhole 128 μm, pixel time 1.28 μs, stack size 1,024 × 1,024 × 1). Ryanodine (25 μM) was added to one chamber of cells and time-lapse confocal microscopy was conducted to assess changes in intracellular Ca^{2+}. F13 (75 μg/ml) was added to a second chamber of cells and changes in intracellular Ca^{2+} were recorded every 5 s for 5 min. Cells earlier exposed to F13 were then challenged with ryanodine (25 μM), and changes in intracellular Ca^{2+} were again recorded every 5 s for 2 min. A second bolus of ryanodine (25 μM) was added to cells 5 min after the first, and changes in intracellular Ca^{2+} were recorded for an additional 3 min. For all assays, Fluo 3 was excited at 488 nm and fluorescence emission was measured at wavelengths >515 nm. Ca^{2+}-release data were analyzed using Image J software (http://rsb.info.nih.gov/nih-image/), Microsoft Excel (Microsoft, Seattle, WA), and Sigma Plot (Systat, Chicago, IL).

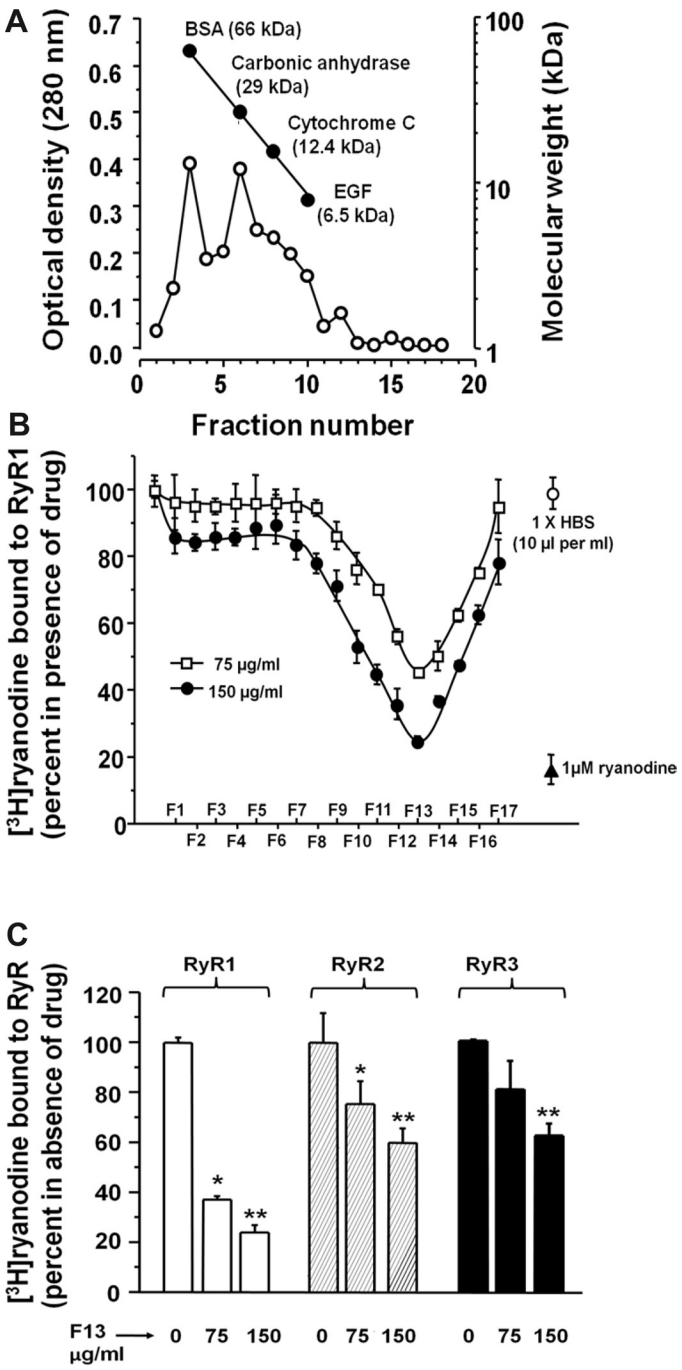

Fig. 1. *A*: representative elution profile of fractions from the Sephadex G-100 column. Fraction 0 was designated as the fraction that eluted from the column immediately after Dextran Blue (M_w 200,000 Da). Phenol red (M_w 354 Da) eluted from the column in fraction 17. *B*: ability of Sephadex G-100 fractions (F1 to F17) to displace [^{3}H]ryanodine binding from RyR1. Data are means ± SEM from five experiments performed in duplicate. Responses to ryanodine as a positive control (open circles) and to the HEPES-buffered saline vehicle as a negative control (closed triangles) are also indicated. *C*: comparison of the ability of 75 and 150 μg/ml F13 to displace [^{3}H]ryanodine from RyR1, RyR2, and RyR3. Data are means ± SEM of four experiments performed using three different samples of HBD. *Significantly different from vehicle control at $P < 0.05$. **Significantly different from 75 μg/ml at $P < 0.05$.

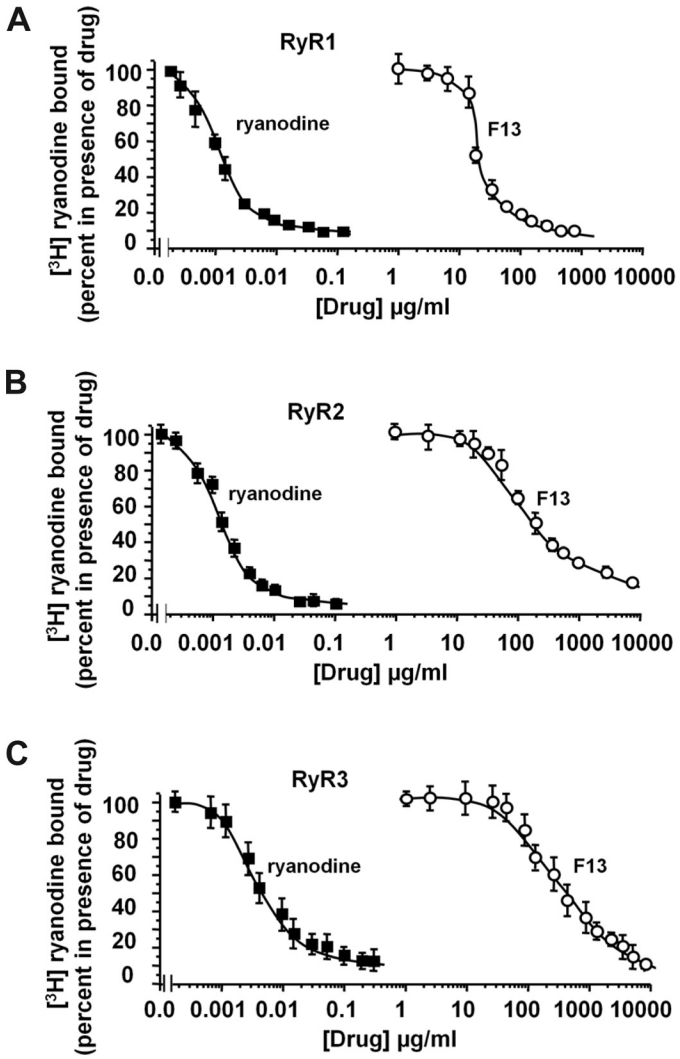

Fig. 2. Relative affinities of HBD (F13) for RyR1, RyR2, and RyR3. Competition of F13 for binding of [^{3}H]ryanodine was assessed in membrane vesicles containing each RyR subtype. Data shown represent means ± SEM from four experiments performed with three different membrane preparations. For comparison, the displacement binding curve for the prototype ligand ryanodine is shown in the closed squares for each panel. *Significantly different from vehicle control at $P < 0.05$.

Effects of F13 on K^+-evoked Ca^{2+} Mobilization from Sarco(endo)plasmic Reticulum

To assess whether F13 impairs depolarization-induced Ca^{2+} release from the SR/ER, C2C12 cells were loaded with 5 μM fura-2 AM in Krebs-Ringer medium containing (in mM) 20 HEPES-Tris pH 7.4, 118 NaCl, 4.7 KCl, 3 $CaCl_2$, 1.2 $MgCl_2$, and 10 glucose for 30 min at 37°C. Cells were then washed three times with fresh Krebs-Ringer to remove extracellular fura-2 and placed on the stage of a Nikon microscope (TE2000) and perfused with Krebs-Ringer solution at a rate of 1.0 ml/min. Depolarization was induced by changing to a Krebs-Ringer solution containing 90 mM KCl with proportionally reduced sodium concentration to maintain osmolarity (in mM: 20 HEPES-Tris pH 7.4, 28 NaCl, 94.7 KCl, 3 $CaCl_2$, 1.2 $MgCl_2$, and 10 glucose) and changes in intracellular Ca^{2+} were measured. After 5 min, cells were again perfused with Krebs-Ringer solution and then incubated for 20 min with F13 (75 μg/ml). Depolarization-induced Ca^{2+} transient was then induced by K^+. All experiments were matched with vehicle-treated controls to eliminate nonspecific effects of F13. Cells were excited at 340/380 nm and emission measured at 510 nm. Recordings were performed using a dual excitation fluorescence photomultiplier system (Image Master Fluorescence Microscope, Photon Technology International, Birmingham, NJ) employing FELIX software.

Statistical Analyses

Data are expressed as means ± SEM. Statistical significance of effects was analyzed using analysis of variance followed by the Bonferroni post-test using Prism 5 (GraphPad Software, San Diego, CA).

RESULTS

Effects of HBD_{aq} fractions on binding of [^{3}H]ryanodine to RyR1, RyR2, and RyR3

Fractions 1–9 of HBD_{aq} obtained from the Sephadex G-100 column (M_w ranging from 200,000 to 10,000 Da) had minimal effect on the binding of [^{3}H]ryanodine to RyR1 (Fig. 1*A*). However, fractions 10–17, which contained compounds of M_w 6,000 to 500 Da, displaced [^{3}H]ryanodine from RyR1 in a Gaussian manner, with fraction 13 (F13), the most active fraction, displacing 50 ± 3% and 80 ± 5% of [^{3}H]ryanodine at 75 μg/ml and 150 μg/ml, respectively (Fig. 1*B*). The HEPES-buffered saline (HBS) used for extraction of HBD had no effect on the binding of [^{3}H]ryanodine to RyR1 (Fig. 1*B*, open circle, top right), whereas the RyR-selective ligand ryanodine (positive control) displaced 92 ± 2% of [^{3}H]ryanodine binding (Fig. 1*B*, filled triangle, bottom right). Similar patterns were obtained using membranes containing RyR2 and RyR3 (data not shown), but F13 was less effective against these isoforms, with 75 μg/ml and 150 μg/ml of HBD displacing ~20% and ~40% of [^{3}H]ryanodine from RyR2 and RyR3, respectively (Fig. 1*C*). Compounds in F13 were estimated to have M_w <2,000 Da.

Table 1. *IC_{50}, K_i, and percent of high-affinity binding sites for F13 binding to RyR1, RyR2, and RyR3 using one- and two-site binding models*

RyR subtype with compound	IC_{50} (μg/ml) one-site model	High-affinity binding sites, one-site model (%)	K_i (μg/ml) one-site model	IC_{50} (μg/ml) two-site model	High-affinity binding sites, two-site model (%)	Ki (μg/ml) two-site model
RyR1						
F13	14.4 ± 1.2	95	3.8 ± 0.2	13.1 ± 1.1 135.1 ± 4.2	89.6	3.5 ± 0.1 35.6 ± 2.7
RyR2						
F13	119.4 ± 5.8	70.1	18.1 ± 2.1	1.1 ± 0.02 125.6 ± 6.5	4.7	0.2 ± 0.01 19.1 ± 2.8
RyR3						
F13	406.2 ± 9.2	79.8	140.6 ± 4.2	128.5 ± 4.5 1434.6 ± 20.2	48.2	44.9 ± 2.8 501.6 ± 9.2

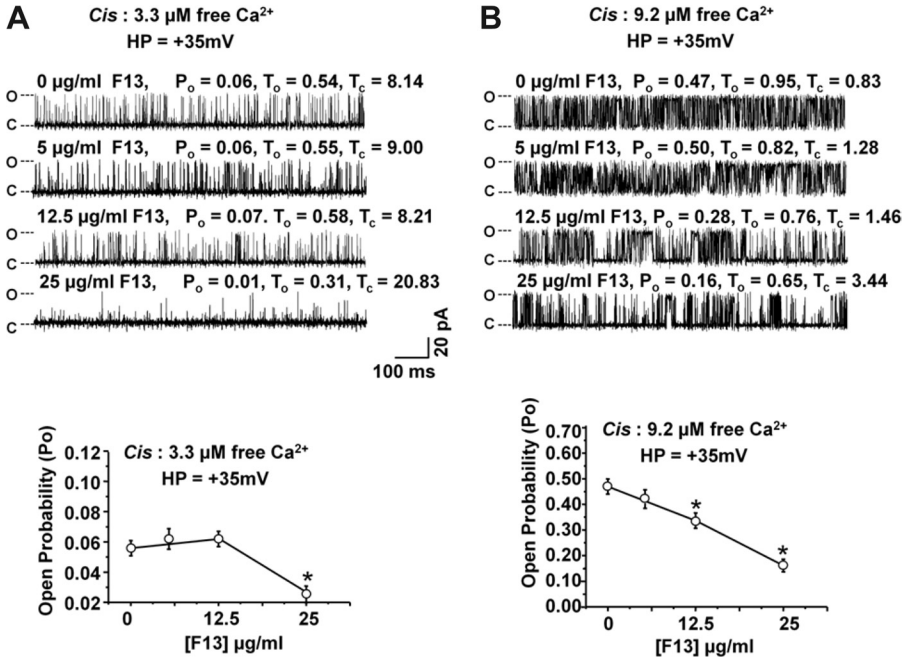

Fig. 3. Functional effects of HBD (F13) on RyR1. *Top:* representative 1-s recordings of RyR1 at +35 mV in the absence and presence of increasing amounts of F13 added to the *cis* chamber for both low channel-opening (left) and high channel-opening (right) conditions in the presence of 3.3 μM *cis* Ca^{2+}. Experiments were conducted in symmetric KCl buffer solution. *Bottom:* means ± SEM for n = 10 channels from two separate RyR1 preparations. *Significantly different from vehicle control at $P < 0.05$.

Affinity of F13 for RyRs

F13 displaced high-affinity [^{3}H]ryanodine binding from RyR1 in a concentration-dependent manner (Fig. 2*A*). The displacement data for F13 fitted well to a one-site binding model, with an IC_{50} value of 14.4 ± 0.1 μg/ml (r^2 = 0.99). The displacement data for F13 also fitted well to a two-site model with 89.6% of sites exhibiting high-affinity binding (IC_{50} = 13.1 ± 1.1 μg/ml) and the remaining sites exhibiting lower-affinity binding (IC_{50} = 135 ± 4 μg/ml). K_i values for F13 on binding to RyR1 were also calculated using the Cheng-Prusoff equation (Table 1). F13 also displaced [^{3}H]ryanodine from RyR2 and RyR3 in a concentration-dependent manner, but displacement data only fitted to a two-site model (Fig. 2, *B* and *C*). IC_{50}, K_i values, and percent of high-affinity binding sites for one- and two-site models are shown in Table 1. The competition curves for the RyR-selective ligand ryanodine are also shown for comparison. Ryanodine exhibited an IC_{50} of 1.6 ± 0.2 ng/ml for RyR1, 0.14 ± 0.01 ng/ml for RyR2, and 2.8 ± 0.1 μg/ml for RyR3).

Effects of F13 on RyR Function

Lipid bilayer assays were used to assess the functional effects of F13 on binding to RyR1, RyR2, and RyR3. F13 (*cis*) reduced the open probability (P_o) of RyR1 regardless of whether channel activity was initially low or high (Fig. 3). The decrease in P_o resulted primarily from a reduction in the number of transitions from the closed to the open state per second (gating frequency), and this effect was independent of holding potential (data not shown), indicating that charged compounds blocking the pore of the channel was not the mechanism for the effects of F13. F13 did not alter the conductance of RyR1. F13 also reduced the open probability of RyR2 and RyR3, but with lower potencies (Fig. 4 and Fig. 5). Effects of F13 on open probability and conductance of RyR1, RyR2, and RyR3 are summarized in Table 2.

Effects of F13 on Ca^{2+} Mobilization from Sarco(endo)plasmic via RyRs in Nonstimulated Cells

Differentiated C2C12 myotubes that express RyR1 and RyR3 (20, 21) were used to assess the functional implications of F13 binding to RyRs. F13 (75 μg/ml) did not elicit any visible change in cytoplasmic Ca^{2+} in Fluo-3-loaded C2C12 cells up to 10 min after addition, suggesting that F13 did not open/activate RyR1/RyR3 (Fig. 6*B*). Similar results were also obtained with 100 μg/ml and 150 μg/ml F13 (data not shown).

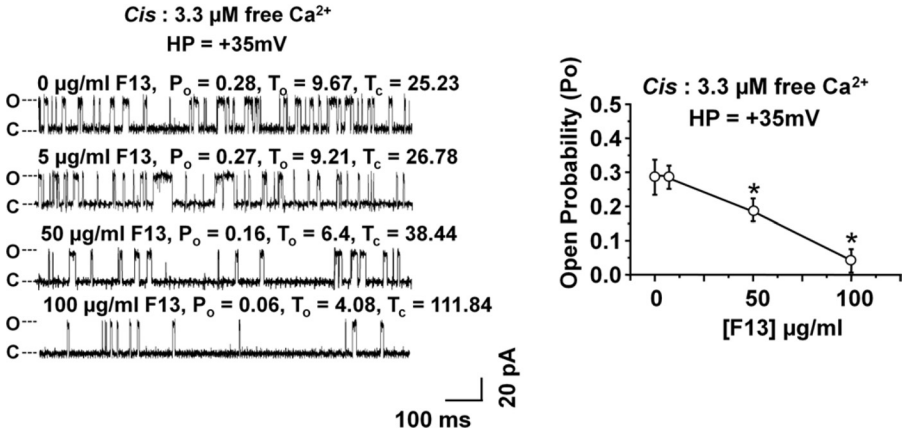

Fig. 4. Functional effects of HBD (F13) on RyR2. *Left*: representative 1-s recordings of RyR2 at +35 mV in the absence and presence of increasing amounts of F13 added to the *cis* chamber with 3.3 μM *cis* Ca^{2+} in the presence of symmetric KCl buffer solution. *Right*: means ± SEM for n = 10 channels from two separate RyR2 preparations. *Significantly different from vehicle control at $P < 0.05$.

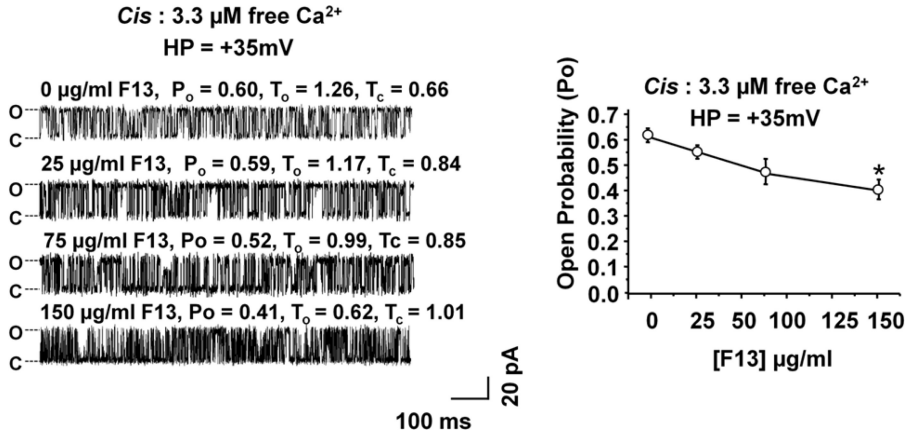

Fig. 5. Functional effects of HBD (F13) on RyR3. *Left*: representative 1-s recordings of RyR2 at +35 mV in the absence and presence of increasing amounts of F13 added to the *cis* chamber with 3.3 μM *cis* Ca^{2+} in the presence of symmetric KCl buffer solution. *Right*: means ± SEM for $n = 10$ channels from two separate RyR2 preparations. *Significantly different from vehicle control at $P < 0.05$.

The ability of F13 to inactivate/close RyR1/RyR3 was tested by assessing its ability to antagonize the action of the RyR-selective agonist ryanodine. Ryanodine (25 μM) elicited Ca^{2+} release from the SR of C2C12 cells within 10 s after addition (Fig. 6*A*). The peak rise in cytoplasmic fluorescence (ΔF) was 3.9 ± 0.2 fluorescence units (f.u) over basal at 20 s after addition of ryanodine and decayed with time (50% after 120 s). However, when C2C12 were pretreated with F13 (75 μg/ml) for 5 min, the amplitude of the Ca^{2+} transient elicited by ryanodine (25 μM) was significantly reduced (ΔF = 0.12 ± 0.03 f.u). A second bolus of ryanodine (25 μM) added 5 min after the first was incapable of eliciting Ca^{2+} release from the SR/ER. Caffeine-evoked Ca^{2+} transient amplitude was also reduced following pretreatment of C2C12 cells with F13 (data not shown). These data are consistent with the notion that F13 is impairing mobilization of Ca^{2+} from the internal sarco-(endo)plasmic reticulum by inhibiting or inactivating RyRs.

Effects of F13 on Evoked Ca^{2+} Mobilization from Sarco(endo)plasmic via RyRs

High extracellular K^+ triggers Ca^{2+} release from the SR/ER via RyRs following activation of voltage-sensitive L-type Ca^{2+}-channels. The amplitude of the K^+-evoked Ca^{2+} transient in cells pretreated with 75 μg/ml of F13 was 36 ± 8%, less than that generated in untreated cells (0.18 ± 0.03 f.u vs. 0.28 ± 0.04 f.u for untreated cells, $n = 12$, $P < 0.05$; Fig. 7). In addition, the rate of rise of intracellular Ca^{2+} was 1.3-fold slower in F13-treated cells than in untreated cells (0.04 ± 0.01 f.u s^{-1} compared with 0.06 ± 0.01 f.u s^{-1} for control, $P < 0.05$). The Ca^{2+} transient decay time was also slower in cells pretreated with F13 than in untreated cells (1.9 ± 0.2 × 10^{-3} f.u s^{-1} vs. 3.5 ± 0.3 × 10^{-3} f.u s^{-1}, respectively; $P < 0.05$).

DISCUSSION

Pig farming is a $20 billion industry in the United States, and continuing national and international demand for pork and pork products is likely to expand this industry even further (52). During the last decade, public discussion/debate on the environmental and health impact of hog CAFOs has led to a reduction in the number of facilities in the United States. However, the CAFOs that remain have enlarged significantly, with some housing in excess 50,000 animals per production cycle (42). This shift toward larger hog CAFOs is raising renewed concerns, as unprecedented amounts of feces, aerobic lagoons, animal carcasses, and bioaerosols are generated and disposed of in localized geographic regions. While many previous studies have indicated a link between the dust generated inside hog confinement facilities and respiratory ailments in facility workers and farm residents, little is known about whether HBD might also be a contributing cause for the increased incidence of nonrespiratory illnesses related to CAFOs, including anger/tension, headaches, depression, skeletal muscle aches and fatigue, nausea, gastrointestinal disorders, and cardiovascular diseases, including heart failure and arrhythmias (11, 16, 17, 24, 40).

The principal finding of the present study is that HBD contains water-soluble compounds of low molecular weight (≤2,000 Da) that impair Ca^{2+} mobilization from internal sarco(endo)plasmic reticulum by inactivating RyRs. These compounds, which were partially purified and concentrated from aqueous extracts of HBD, are extremely potent, exhibiting affinities of ≤50 μg/ml for

Table 2. *Effects of F13 on the open probability of RyR1, RyR2 and RyR3*

RyR subtype	[F13] (μg/ml)	*cis* [Ca^{2+}] (μM)	Open Probability (P_o)	Dwell time opened state (ms)	Dwell time closed state (ms)	Transitions per second from close to open state	Conductance (G) pS
RyR1	0	3.3	0.06 ± 0.01	0.52 ± 0.1	8.11 ± 0.92	114 ± 8	750 ± 10
	25		0.01 ± 0.00*	0.31 ± 0.01*	20.86 ± 1.24*	67 ± 9*	776 ± 12
	0	9.2	0.47 ± 0.03	0.95 ± 0.15	0.83 ± 0.14	579 ± 16	749 ± 9
	25		0.16 ± 0.02*	0.07 ± 0.01*	3.42 ± 0.43	266 ± 11*	768 ± 11
RyR2	0	3.3	0.28 ± 0.02	9.62 ± 0.70	25.26 ± 5.23	33 ± 7	670 ± 5
	100		0.06 ± 0.01*	4.07 ± 0.50*	111.92 ± 10.11*	10 ± 2*	676 ± 6
RyR3	0	3.3	0.60 ± 0.05	1.33 ± 0.11	0.73 ± 0.13	136 ± 7	643 ± 10
	150		0.41 ± 0.02*	0.63 ± 0.11*	1.15 ± 0.14*	80 ± 8*	649 ± 11

*Significantly different from no drug (0 μg/ml).

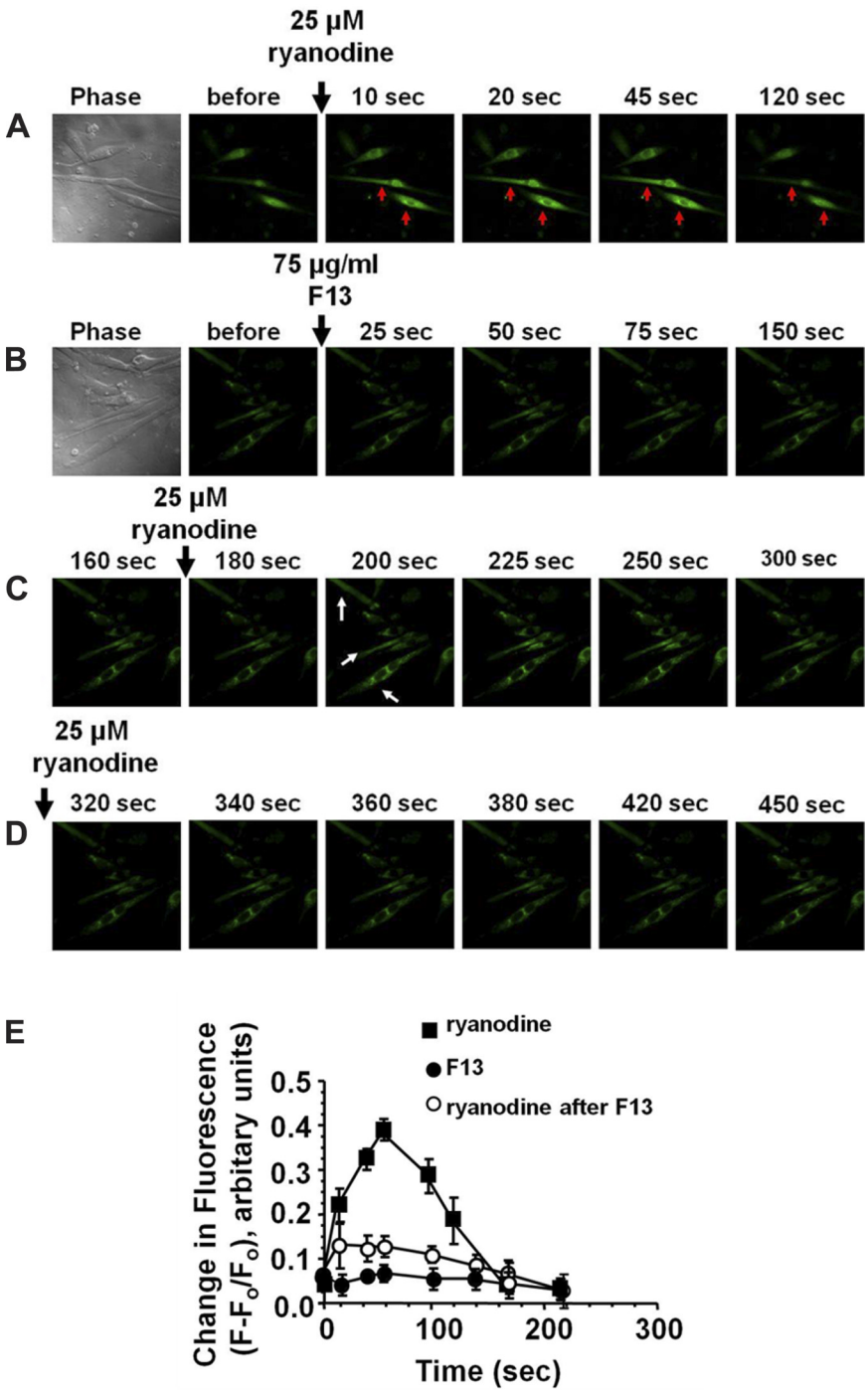

Fig. 6. F13 impairs mobilization of Ca^{2+} from internal stores in quiescent cells. *A*: representative time-lapse confocal recording showing changes in intracellular Ca^{2+} of C2C12 cells challenged with 25 μM ryanodine. Red arrows indicate changes in intracellular Ca^{2+}. *B*: representative time-lapse recording showing changes in intracellular Ca^{2+} of C2C12 cells challenged with 75 μg/ml F13. *C*: representative time-lapse recording showing changes in intracellular Ca^{2+} of C2C12 cells pretreated with 75 μg/ml F13 and then challenged with 25 μM ryanodine. White arrows indicate changes in intracellular Ca^{2+}. *D*: representative time-lapse recording showing changes in intracellular Ca^{2+} of C2C12 cells pretreated with 75 μg/ml F13 and challenged with a second bolus of ryanodine (25 μM). *E*: Ca^{2+} transients recorded over 200 s (mean ± SEM) for six separate experiments.

RyR1, RyR2, and RyR3. Analysis of the high-affinity [^{3}H]ryanodine displacement binding curves suggests that HBD is interacting with more than one site on RyR1, RyR2, and RyR3. Whether the multiple binding sites are due to multiple compounds in F13 exhibiting different binding affinities, or to one compound binding to two distinct sites, remains to be resolved.

In a previous study, we found that chloroform extracts of HBD contain organic compounds that bind to and biphasically activate and then inhibit RyR1 (48). The water-soluble compounds present in F13 are functionally distinct from those in the chloroform extracts, because there is no evidence that F13 activated RyRs; rather, it inhibited RyRs. Further fractionation of F13 will be required to establish the identities of the RyR-active compounds in the chloroform and aqueous extracts and to determine whether they are peptides, microbial metabolites, or molecules derived from chemical reactions taking place inside CAFOs.

In lipid bilayer assays, F13 dose-dependently reduced the open probability of RyR1, RyR2, and RyR3 without altering their conductances. F13 was also more efficacious in inactivating RyR1 than RyR2, or RyR3. Because RyR1 is predominant in skeletal muscles, and inactivation uncouples it from L-type

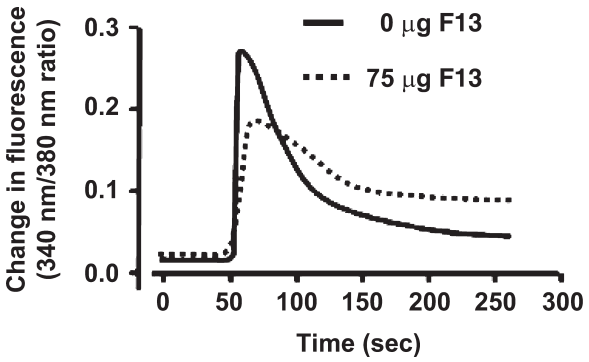

Fig. 7. F13 impairs K^+-evoked Ca^{2+} mobilization from internal stores. Representative K^+-induced $[Ca^{2+}]_i$ transients in C2C12 cells pretreated and not pretreated with F13 (75 μg/ml). C2C12 cells were loaded with fura 2-AM for 30 min. After loading, cells were washed, transferred to a perfusion chamber mounted on the stage of an inverted microscope, and perfused with Krebs-Ringer solution. Depolarization was then evoked by KCl (90 mM) and changes in intracellular Ca^{2+} were measured. After 5 min, cells were again perfused with Krebs-Ringer solution and then incubated for 20 min with F13 (75 μg/ml). After this time, depolarization-induced Ca^{2+} transient was induced by K^+. Mean amplitudes for Ca^{2+} transients, rate of rise of Ca^{2+} release, and rate of Ca^{2+} transient decay are listed in the text. Experiments were repeated four times with two separate cell preparation.

Ca^{2+} channels, these data reinforce the notion that HBD contains compounds, both lipid- and aqueous-soluble, that impair mobilization of Ca^{2+} from the sarco(endo)plasmic reticulum by inactivating RyRs (13, 48).

Our data show that F13 also binds with high affinity and inhibits RyR2, the major RyR isoform present in heart and brain. This is an important finding that could provide new insights regarding the exacerbation of cardiovascular diseases such as heart failure, arrhythmias, headaches, and nausea reported by confinement facility workers and individuals living in surrounding communities. Cardiac contractions depend critically on the timely, adequate, and synchronized release of Ca^{2+} from the SR via RyR2. Following depolarization, a small amount of extracellular Ca^{2+} enters cardiac myocytes via L-type Ca^{2+} channels. This Ca^{2+} binds to and activates/opens RyR2, a process known as Ca^{2+}-induced Ca^{2+} release. If RyR2 becomes unresponsive to the elevated intracellular Ca^{2+}, then the amount of Ca^{2+} release from the SR would be reduced, thereby negatively impacting cardiac contractions. Uncoordinated or delayed opening of RyR2 could also trigger delayed-after-depolarization and arrhythmias (51, 54).

RyR2 is also the major RyR isoform in the brain, where it plays important roles in presynaptic neurotransmitter release, gene transcription, and the postsynaptic plasticity that underpins cognitive function (53, 55, 56). Under basal conditions, neuronal intracellular Ca^{2+} is in the nM range, but upon electrical or ligand-induced stimulation, Ca^{2+} rises to μM concentrations in a precise and timely manner within specific regions to elicit the desired effect (2). The majority of Ca^{2+} needed for executing these functions is recruited from the ER via RyR2. Inactivation by HBD would reduce the amplitudes of these responses and thus could elicit observed effects such as headaches and nausea. Headaches are seen as side effects with the prostacyclin analog beraprost sodium, which also inhibits Ca^{2+} release from intracellular stores (35). F13 also binds to and inhibits RyR3, but with reduced efficacy compared with RyR1 and RyR2. Because RyR3 plays important roles in regulating smooth muscle, particularly vascular tone and gastrointestinal mobility (12), these findings could implicate RyR3 modulation by HBD as an underlying cause for the increased gastrointestinal distress reported by confinement facility workers and individuals living in close proximity to CAFOs.

Pretreatment with F13 attenuated the ability of the RyR-selective agonist ryanodine to mobilize Ca^{2+} from the intracellular stores in quiescent C2C12 cells. Pretreatment with F13 also attenuated evoked Ca^{2+} release from C2C12 cells. These effects were observed by pretreating cells with as little as 25 μg/ml F13 for 5 min but were more robust with 75 μg/ml HBD. To put these data into context, the emission rate of respirable dust from hog CAFOs is estimated to be 60 mg·h·500 kg per live animal. For a CAFO with 50,000 hogs of 25 kg each, 150 g of dust per hour (42) will be emitted. In our study, 1 g of HBD was extracted with 10 ml of buffer and 2.5 ml of the extract was separated on Sephadex G-100 resin into 17 fractions. Assuming equivalent masses in each fraction, F13 would contain 15 μg of RyR-active compounds. Thus the amount of RyR-active compounds emitted into the environment in the form of dust from hog CAFOs over the 3- to 4-mo growing period is enormous.

Although the use of C2C12 cells established the proof of concept that HBD can impair Ca^{2+} release from the SR/ER, our study is not without limitations. First, C2C12 cells express both RyR1 and RyR3 isoforms (20, 21), and the relative contribution of each RyR isoform in preventing Ca^{2+} release express from the SR/ER remains uncertain. C2C12 cells also express IP_3Rs (5), and IP_3R blockers (e.g., xestospongins) were not used in studies investigating Ca^{2+} release in quiescent cells. Additional studies are ongoing using L6 skeletal muscle myotubes that express RyR1, rat ventricular myocytes that express RyR2, HEK-293T cells transfected with recombinant mouse cDNA encoding RyR3 (a gift from Dr. S.R.W. Chen, University of Alberta), and with IP_3R blockers to better delineate the effects of HBD on evoked Ca^{2+} release from the SR/ER. Second, pretreatment of C2C12 cells with F13 reduced ryanodine- and K^+-induced Ca^{2+} release from the SR/ER, and this was attributed in part to inhibition of RyRs. However, a reduction in Ca^{2+} transient amplitude could also result from a reduction in activity of sarco(endo)plasmic reticulum Ca^{2+}-ATPase (SERCA), the ATP-dependent pump that translocates Ca^{2+} from the cytoplasm to the lumen of the SR/ER. The slowing in the Ca^{2+} transient decay in Fig. 7 (broken line) suggests that this might be the case. More work is therefore needed to address effects of HBD on the activity of SERCA.

In summary, the present study shows for the first time that the dust generated inside hog CAFOs contains compounds that impair mobilization of Ca^{2+} from internal sarco(endo)plasmic reticulum by inhibiting all three isoforms of RyR. The inability of RyRs to open and release Ca^{2+} from internal stores could significantly impair physiologic responses of cells and trigger adverse effects such as muscle aches/fatigue, nausea, diarrhea, headaches, and cardiovascular diseases, akin to the complaints reported by hog CAFO workers and residents in close proximity to these facilities. These nonrespiratory illnesses have been presumed to be secondary to respiratory illness, as a consequence of breathing toxic gases such as hydrogen sulfide, ammonia, and methane generated by CAFOs, and from particulate matter less than 10 μm in diameter. Our findings suggest yet another mechanism that could account for these illnesses; namely, impairment of Ca^{2+} mobilization from internal stores. It is possible that even the respiratory ailments in hog CAFO workers and residents in immediate vicin-

ity could be due in part to HBD inactivating RyRs on various types of lung cells. Further studies to identify the specific component(s) of HBD that bind and modulate RyRs could lead to a better understanding of their mechanisms of action and their physiologic/pathophysiologic relevance. They could also lead to approaches to monitor their environmental concentrations and toxicity and to reduce and treat the diverse array of HBD-associated pathologies.

GRANTS

This work was supported in part by National Heart, Lung, and Blood Institute Grant HL085061 to K.R.B. and by National Institute of Occupational Safety and Health Grant OH008539 to D.J.R.

DISCLOSURES

No conflicts of interest, financial or otherwise, are declared by the author(s).

AUTHOR CONTRIBUTIONS

Author contributions: C.T., C.J.M., P.D., and C.H.S. performed experiments; C.T., C.J.M., P.D., C.H.S., and K.R.B. analyzed data; C.T., C.J.M., P.D., C.H.S., M.L.T., and K.R.B. interpreted results of experiments; C.T., C.J.M., C.H.S., and K.R.B. prepared figures; C.T., C.J.M., P.D., C.H.S., D.J.R., M.L.T., and K.R.B. approved final version of manuscript; C.J.M., D.J.R., M.L.T., and K.R.B. edited and revised manuscript; D.J.R., M.L.T., and K.R.B. conceived and designed research; K.R.B. drafted manuscript.

REFERENCES

1. **Bailey KL, Poole JA, Mathisen TL, Wyatt TA, Von Essen SG, Romberger DJ.** Toll-like receptor 2 is upregulated by hog confinement dust in an IL-6-dependent manner in the airway epithelium *Am J Physiol Lung Cell Mol Physiol* 294: L1049–L1054, 2008.
2. **Berridge MJ, Bootman MD, Roderick HL.** Calcium signalling: dynamics, homeostasis and remodelling. *Nat Rev Mol Cell Biol* 4: 517–529, 2003.
3. **Berridge MJ.** The versatility and complexity of calcium signalling. *Novartis Found Symp* 239: 52–64, 2001.
4. **Bers DM.** Cardiac excitation-contraction coupling. *Nature* 415: 198–205, 2002.
5. **De Smedt H, Missiaen L, Parys JB, Bootman MD, Mertens L, Van den Bosch L, Casteels R.** Determination of relative amounts of inositol trisphosphate receptor mRNA isoforms by ratio polymerase chain reaction. *J Biol Chem* 269: 21691–21698, 1994.
6. **Bezprozvanny I, Watras J, Ehrlich BE.** Bell-shaped calcium-response curves of Ins(1,4,5)P3- and calcium-gated channels from endoplasmic reticulum of cerebellum. *Nature* 351: 751–754, 1991.
7. **Bidasee KR, Xu L, Meissner G, Besch HR Jr.** Diketopyridylryanodine has three concentration-dependent effects on the cardiac calcium-release channel/ryanodine receptor. *J Biol Chem* 278: 14237–14248, 2003.
8. **Bunton B, O'shaughnessy P, Fitzsimmons S, Gering J, Hoff S, Lyngbye M, Thorne PS, Wasson J, Werner M.** Monitoring and modeling of emissions from concentrated animal feeding operations: overview of methods. *Environ Health Perspect* 115: 303–307, 2007.
9. **Chapin A, Boulind C, Moore A.** *Controlling odor and gaseous emission problems from industrial swine facilities (a handbook for all interested parties)* (Online). Yale Environmental Protection Clinic; 1998. http://www.kerrcenter.com/publications/hogodor_laws.pdf.
10. **Chen C, Okayama H.** High-efficiency transformation of mammalian cells by plasmid DNA. *Mol Cell Biol* 7: 2745–2752, 1997.
11. **Cormier Y, Israël-Assayag E.** Chronic inflammation induced by organic dust and related metabolic cardiovascular disease risk factors. *Scand J Work Environ Health* 30: 438–444, 2004.
12. **Dabertrand F, Mironneau J, Macrez N, Morel JL.** Full length ryanodine receptor subtype 3 encodes spontaneous calcium oscillations in native duodenal smooth muscle cells. *Cell Calcium* 44: 180–189, 2008.
13. **Dirksen RT, Avila G.** Altered ryanodine receptor function in central core disease: leaky or uncoupled Ca(2+) release channels? *Trends Cardiovasc Med* 12: 189–197, 2002.
14. **Dodmane PR, Schulte NA, Heires AJ, Band H, Romberger DJ, Toews ML.** Airway epithelial epidermal growth factor receptor mediates hogbarn dust-induced cytokine release but not Ca^{2+} response. *Am J Respir Cell Mol Biol* 45: 882–888, 2011.
15. **Donham KJ, Popendorf W, Palmgren U, Larsson L.** Characterization of dusts collected from swine confinement buildings. *Am J Ind Med* 10: 294–297, 1986.
16. **Donham KJ.** Community and occupational health concerns in pork production: a review. *J Anim Sci* 88(13 *Suppl*): E102–E111, 2010.
17. **Donham KJ.** Health effects from work in swine confinement buildings. *Am J Ind Med* 17: 17–25, 1990.
18. **Dulhunty AF, Pouliquin P.** What we don't know about the structure of ryanodine receptor calcium release channels. *Clin Exp Pharmacol Physiol* 30: 713–723, 2003.
19. **Giannini G, Sorrentino V.** Molecular structure and tissue distribution of ryanodine receptors calcium channels. *Med Res Rev* 15: 313–323, 1995.
20. **Grassi F, Giovannelli A, Fucile S, Eusebi F.** Activation of the nicotinic acetylcholine receptor mobilizes calcium from caffeine-insensitive stores in C2C12 mouse myotubes. *Pflugers Arch* 422: 591–598, 1993.
21. **Henning RH, Duin M, Den Hertog A, Nelemans A.** Activation of the phospholipase C pathway by ATP is mediated exclusively through nucleotide type P2-purinoceptors in C2C12 myotubes. *Br J Pharmacol* 110: 747–752, 1993.
22. **Hribar C.** *Understanding concentrated animal feeding operations and their impact on communities* (Online). National Association of Local Boards of Health; 2010. http://www.cdc.gov/nceh/ehs/Docs/Understanding_CAFOs_NALBOH.pdf [14 May 2012].
23. **Iowa State University and The University of Iowa Study Group.** *Iowa concentrated animal feeding operations air quality study* (Online). http://www.public-health.uiowa.edu/ehsrc/CAFOstudy/CAFO_final2–14.pdf [14 May 2012].
24. **Iowa State University.** *National Agricultural Safety database, livestock confinement dusts, and ga* http://nasdonline.org/document/1627/d001501/livestock-confinement-dust-and-gases.html [6 May 2012].
25. **Iversen M, Dahl R.** Working in swine-confinement buildings causes an accelerated decline in FEV1: a 7-yr follow-up of Danish farmers. *Eur Respir J* 16: 404–408, 2000.
26. **Kelliher M, Fastbom J, Cowburn RF, Bonkale W, Ohm TG, Ravid R, Sorrentino V, O'Neill C.** Alterations in the ryanodine receptor calcium release channel correlate with Alzheimer's disease neurofibrillary and beta-amyloid pathologies. *Neuroscience* 92: 499–513, 1999.
27. **Ko G, Simmons OD III, Likirdopulos CA, Worley-Davis L, Williams M, Sobsey MD.** Investigation of bioaerosols released from swine farms using conventional and alternative waste treatment and management technologies. *Environ Sci Technol* 42: 8849–8857, 2008.
28. **Koelsch R.** Evaluating livestock system environmental performance with whole-farm nutrient balance. *J Environ Qual* 34: 149–155, 2005.
29. **Kushnir A, Marks AR.** The ryanodine receptor in cardiac physiology and disease. *Adv Pharmacol* 59: 1–30, 2010.
30. **Larsson KA, Eklund AG, Hansson LO, Isaksson BM, Malmberg PO.** Swine dust causes intense airways inflammation in healthy subjects. *Am J Respir Crit Care Med* 150: 973–977, 1994.
31. **MacKrill JJ.** Protein-protein interactions in intracellular Ca2+-release channel function. *Biochem J* 337: 345–361, 1999.
32. **Malmberg P, Larsson K.** Acute exposure to swine dust causes bronchial hyperresponsiveness in healthy subjects. *Eur Respir J* 6: 400–404, 1993.
33. **Mathisen T, Von Essen SG, Wyatt TA, Romberger DJ.** Hog barn dust extract augments lymphocyte adhesion to human airway epithelial cells. *J Appl Physiol* 96: 1738–1744, 2004.
34. **McElroy KG.** Environmental health effects of concentrated animal feeding operations: implications for nurses. *Nurs Adm Q* 34: 311–319, 2010.
35. **Melian EB, Goa KL.** Beraprost: a review of its pharmacology and therapeutic efficacy in the treatment of peripheral arterial disease and pulmonary arterial hypertension. *Drugs* 62: 107–133, 2002.
36. **Motulsky H, Christopoulos A.** *Analyzing data with GraphPad Prism*. San Diego, CA: GraphPad Software Inc., 2005.
37. **National Research Council.** *Guide for the Care and Use of Laboratory Animals*. Washington, DC: National Academy Press, 1996.
38. **Poole JA, Wyatt TA, Oldenburg PJ, Elliott MK, West WW, Sisson JH, Von Essen SG, Romberger DJ.** Intranasal organic dust exposure-induced airway adaptation response marked by persistent lung inflammation and pathology in mice. *Am J Physiol Lung Cell Mol Physiol* 296: L1085–L1095, 2009.
39. **Romberger DJ, Bodlak V, Von Essen SG, Mathisen T, Wyatt TA.** Hog barn dust extract stimulates IL-8 and IL-6 release in human bronchial epithelial cells via PKC activation. *J Appl Physiol* 93: 289–296, 2002.

40. **Schiffman SS, Miller EA, Suggs MS, Graham BG.** The effect of environmental odors emanating from commercial swine operations on the mood of nearby residents. *Brain Res Bull* 37: 369–375, 1995.
41. **Schwartz DA, Donham KJ, Olenchock SA, Popendorf WJ, Van Fossen DS, Burmeister LF, Merchant JA.** Determinants of longitudinal changes in spirometric function among swine confinement operators and farmers. *Am J Respir Crit Care Med* 151: 47–53, 1995.
42. **Seedorf J, Hartung J.** *Emission of airborne particulates from animal production. Sustainable Animal Production: Conference, Workshops, Discussion* (Online). http://www.agriculture.de/acms1/conf6/ws4dust.htm?&template=/acms1/conf6/tpl/print.tpl. [6 March 2012].
43. **Skeie GO, Romi F, Aarli JA, Bentsen PT, Gilhus NE.** Pathogenesis of myositis and myasthenia associated with titin and ryanodine receptor antibodies. *Ann N Y Acad Sci* 998: 343–350, 2003.
44. **Slager RE, Allen-Gipson DS, Sammut A, Heires A, DeVasure J, Von Essen S, Romberger DJ, Wyatt TA.** Hog barn dust slows airway epithelial cell migration in vitro through a PKCα-dependent mechanism. *Am J Physiol Lung Cell Mol Physiol* 293: L1469–L1474, 2007.
45. **Starmer E.** *Agricultural Business Initiative: Environmental and Health Problems in Livestock Production: Pollution in the Food System Issue Brief #2* (Online). The Agribusiness Accountability Initiative; 2007. http://www.ase.tufts.edu/gdae/Pubs/rp/AAI_Issue_Brief_2_1.pdf [6 May 2012].
46. **Szadkowska-Stańczyk I, Bródka K, Buczyńska A, Cyprowski M, Kozajda A, Sowiak M.** Exposure to bioaerosols among CAFO workers (swine feeding). *Med Pr* 61: 257–269, 2010.
47. **Thu KM.** Public health concerns for neighbors of large-scale swine production operations. *J Agric Saf Health* 8: 175–184, 2002.
48. **Tian C, Shao CH, Fenster DS, Mixan M, Romberger DJ, Toews ML, Bidasee KR.** Chloroform extract of hog barn dust modulates skeletal muscle ryanodine receptor calcium-release channel (RyR1). *J Appl Physiol* 109: 830–839, 2010.
49. **Tian C, Shao CH, Moore CJ, Kutty S, Walseth T, DeSouza C, Bidasee KR.** Gain of function of cardiac ryanodine receptor in a rat model of type 1 diabetes. *Cardiovasc Res* 91: 300–309, 2011.
50. **Von Essen SG, Auvermann BW.** Health effects from breathing air near CAFOs for feeder cattle or hogs. *J Agromedicine* 10: 55–64, 2005.
51. **Watanabe H, Knollmann BC.** Mechanism underlying catecholaminergic polymorphic ventricular tachycardia and approaches to therapy. *J Electrocardiol* 44: 650–655, 2011.
52. **WattAgNet.com.** *WattAgNet.com* (Online). Watt Publishing Co. http://www.wattagnet.com [May 2012].
53. **Wojda U, Salinska E, Kuznicki J.** Calcium ions in neuronal degeneration. *IUBMB Life* 60: 575–590, 2008.
54. **Yano M, Yamamoto T, Kobayashi S, Matsuzaki M.** Role of ryanodine receptor as a Ca(2+) regulatory center in normal and failing hearts. *J Cardiol* 53: 1–7, 2009.
55. **Yuste R, Majewska A, Holthoff K.** From form to function: calcium compartmentalization in dendritic spines. *Nat Neurosci* 3: 653–659, 2000.
56. **Zhuang SY, Bridges D, Grigorenko E, McCloud S, Boon A, Hampson RE, Deadwyler SA.** Cannabinoids produce neuroprotection by reducing intracellular calcium release from ryanodine-sensitive stores. *Neuropharmacology* 48: 1086–1096, 2005.